Bone 133 (2020) 115266

Contents lists available at ScienceDirect

Bone

journal homepage: www.elsevier.com/locate/bone

Full Length Article

Pulsed electromagnetic fields modify the adverse effects of glucocorticoids on bone architecture, bone strength and porous implant osseointegration by rescuing bone-anabolic actions

Jing Cai[a,b,1], Xi Shao[b,1], Qiuju Yang[c], Yongqing Yang[b], Zedong Yan[b], Erping Luo[b], Xue Feng[d,*], Da Jing[b,**]

[a] College of Basic Medicine, Shaanxi University of Chinese Medicine, Xianyang, China
[b] Department of Biomedical Engineering, Fourth Military Medical University, Xi'an, China
[c] Department of Anesthesia, The First Clinical College, Xinxiang Medical University, Xinxiang, China
[d] Department of Cell Biology, School of Medicine, Northwest University, Xi'an, China

ARTICLE INFO

Keywords:
Glucocorticoids
Pulsed electromagnetic fields (PEMF)
Osteoporosis
Implant osseointegration
Bone anabolism
Canonical Wnt signaling

ABSTRACT

Long-term glucocorticoid therapy is known to induce increased bone fragility and impaired skeletal regeneration potential. Growing evidence suggests that pulsed electromagnetic fields (PEMF) can accelerate fracture healing and increase bone mass both experimentally and clinically. However, how glucocorticoid-treated bone and bone cells respond to PEMF stimulation remains poorly understood. Here we tested the effects of PEMF on bone quantity/quality, bone metabolism, and porous implant osseointegration in rabbits treated with dexamethasone (0.5 mg/kg/day, 6 weeks). The micro-CT, histologic and nanoindentation results showed that PEMF ameliorated the glucocorticoid-mediated deterioration of cancellous and cortical bone architecture and intrinsic material properties. Utilizing the new porous titanium implant (Ti2448) with low toxicity and low elastic modulus, we found that PEMF stimulated bone ingrowth into the pores of implants and enhanced peri-implant bone material quality during osseous defect repair in glucocorticoid-treated rabbits. Dynamic histomorphometric results revealed that PEMF reversed the adverse effects of glucocorticoids on bone formation, which was confirmed by increased circulating osteocalcin and P1NP. PEMF also significantly attenuated osteocyte apoptosis, promoted osteoblast-related osteocalcin, Runx2 and Osx expression, and inhibited osteocyte-specific DKK1 and Sost expression (negative regulators of osteoblasts) in glucocorticoid-treated skeletons, revealing improved functional activities of osteoblasts and osteocytes. Nevertheless, PEMF exerted no effect on circulating bone-resorbing cytokines (serum TRAcP5b and CTX-1) or skeletal gene expression of osteoclast-specific markers (TRAP and cathepsin K). PEMF also significantly upregulated skeletal gene expression of canonical Wnt ligands (Wnt1, Wnt3a and Wnt10b), whereas PEMF did not alter non-canonical Wnt5a expression. This study demonstrates that PEMF treatment improves bone mass, strength and porous implant osseointegration in glucocorticoid-treated rabbits by promoting potent bone-anabolic action, which is associated with canonical Wnt-mediated improvement in osteoblast and osteocyte functions. This study provides a new treatment alternative for glucocorticoid-related bone disorders in a convenient and non-invasive manner.

1. Introduction

The therapeutic use of glucocorticoids (GC) remains an important approach for a wide range of chronic inflammatory and autoimmune diseases in clinics, such as asthma, organ transplants, inflammatory bowel diseases and rheumatoid arthritis [1]. However, prolonged administration of GC has proven detrimental to various organs and tissues, especially to the skeletal system [2]. Chronic exposure to GC is found to induce a profound reduction in bone quantity and/or quality, subsequently increasing the risks of fragility fractures and osteonecrosis [3–5]. It has been reported that almost 50% of patients treated with GC suffer from a traumatic fracture throughout their lives, and GC therapy

* Correspondence to: X. Feng, School of Medicine, Northwest University, 229 Taibai North Road, Xi'an 710069, China.
** Correspondence to D. Jing, Department of Biomedical Engineering, Fourth Military Medical University, 17 West Changle Road, Xi'an 710032, China.
E-mail addresses: prof.fengxue@outlook.com (X. Feng), jingdaasq@126.com (D. Jing).
[1] These authors contributed equally to this work.

https://doi.org/10.1016/j.bone.2020.115266
Received 29 October 2019; Received in revised form 5 February 2020; Accepted 6 February 2020
Available online 07 February 2020
8756-3282/

is regarded as the leading cause of secondary osteoporosis [5–7]. GC can also delay bone healing and impair skeletal regeneration potential and osseointegration of various implants [8,9]. Although the etiology has not yet been fully elucidated, compromised osteoblast differentiation and function and increased apoptosis of osteoblasts and osteocytes are considered to be the major mechanism of GC-induced bone deterioration [5,10–12]. Thus, anti-osteoporotic treatments that can promote bone anabolism may be especially beneficial for resisting GC-related bone disorders. It has been reported that bone anabolic therapy by parathyroid hormone (PTH) or PTH-related protein (PTHrP) effectively inhibited GC-induced bone loss [13–15]. Recent studies have shown that sclerostin antibody, another potential anabolic agent, also preserved bone mass in GC-treated rodents [16,17]. However, the potential side effects and high cost of these drugs may limit their extensive clinical application, especially in developing countries and regions. Thus, further work is needed to develop economic and safe anabolic therapies for GC-associated bone deficits in the clinic.

Since the discovery of bone's piezoelectric properties in the 1950s, the biological consequence of exogenous electrical/magnetic signals on bone has attracted extensive attention. Subsequent studies revealed that electrical stimulation was able to promote osteogenesis [18,19]. Bassett was the first to show the positive effects of non-contact pulsed electromagnetic fields (PEMF) on delayed and non-union fractures [20], and the safety and effectiveness of PEMF in clinical orthopedic applications were approved by the FDA in 1979. Subsequent studies confirm the therapeutic benefits of PEMF on various bone disorders both experimentally and clinically, such as fractures, bone defects, osteoarthritis and spinal cord injury [21–25]. In particular, recent accumulating evidence suggests that PEMF can raise bone mass and enhance bone strength in osteoporotic animals induced by ovariectomy, disuse, or diabetes [24–28]. Several clinical trials have also demonstrated that PEMF treatment increases bone mineral density (BMD) in postmenopausal women [29,30]. Despite the growing body of knowledge about the skeletal benefits of PEMF, the potential effects and regulatory mechanisms of PEMF in the treatment of GC-related bone loss and bone injury remain poorly understood.

Substantial evidence has revealed the essential role of canonical Wnt (Wnt/β-catenin) signaling in the regulation of bone modeling and remodeling [31]. It has been reported that GC exposure suppresses the activation of the canonical Wnt signaling pathway [32]. It has been shown that PEMF treatment stimulates the activation of canonical Wnt signaling in osteoblasts *in vitro* [33]. The skeletal molecule expression levels of canonical Wnt signaling are also significantly upregulated in normal or ovariectomized animals under PEMF stimulation [34,35]. Furthermore, growing evidence has also suggested that non-canonical Wnt (β-catenin independent) signaling is important for mediating bone metabolism and homeostasis [36]. In this context, it is interesting to investigate whether the canonical and non-canonical Wnt pathways are implicated in PEMF-mediated regulation of bone metabolism and structure in the GC-induced osteoporotic model.

In this study, the therapeutic effects of PEMF on bone mass, architecture, and biomechanical properties of cancellous and cortical bone in GC-treated rabbits were investigated. Based on our previously developed non-toxic Ti2448 porous titanium alloy (pTi) with similarly high strength and greatly reduced elastic modulus (more similar to the elastic modulus of natural bone) compared with the traditional Ti-6Al-4V alloy [26], we also evaluated the impacts of PEMF on bone defect regeneration and implant osseointegration in GC-treated rabbits. Moreover, the mechanisms, by which PEMF regulated bone metabolism as well as the functional activities of bone cells (*i.e.*, osteoblasts, osteoclasts and osteocytes) in GC-treated rabbits, were also investigated.

2. Materials and methods

2.1. Porous titanium implants

The detailed fabrication process of the Ti2448 pTi implants has been described in our previous study [26]. In brief, computer-aided design (CAD) software was employed to design the pTi model, and the structural parameters were designed as follows: diameter 6.0 mm, length 8.0 mm, porosity 70%, and pore size 750 μm. The Ti2448 alloy powder, a novel β-type titanium alloy comprising non-toxic compositions of 24.1% niobium, 3.92% zirconium, 7.85% stannum and 64% titanium, was cast into the Ti2448 pTi implants using an electron beam melting system (EBM S12, Acram AB, Sweden) based on the CAD model. The elastic modulus of the Ti2448 material with the ageing treatment in the hexagonal close-packed (α) + body-centered cubic (β) two-phase field is ~30 GPa [37], which is much closer to the modulus of human bone (10–20 GPa) than that of the commercial Ti-6Al-4V alloy (> 100 GPa) [38]. The pTi implants were imaged using a scanning electron microscope (SEM, JSM-6460, JEOL, Japan) to provide gross visual information of the three-dimensional morphological features of the implant.

2.2. Animals and study design

The overall experimental protocol is shown in Fig. 1. Twenty-four male New Zealand rabbits (purchased from the Animal Center of the Fourth Military Medical University), 21.2 ± 1.4 weeks of age weighing 3.4 ± 0.5 kg, were used. Following 1 week of acclimatization to the laboratory, rabbits were randomly divided into three equal groups (n = 8), including the blank control rabbits (Control), glucocorticoid-treated rabbits (GC), and glucocorticoid-treated rabbits with PEMF exposure (PEMF). The animals in the GC and PEMF groups were subcutaneously injected with 0.5 mg/kg dexamethasone per day for 6 consecutive weeks. This concentration of dexamethasone has proven to be effective at inducing significant bone loss in animals [39,40]. The rabbits in the Control group were subcutaneously injected with sterile saline as the sham control. After dexamethasone injection for 1 week, the bone defect model was surgically established in all rabbits according to the procedures reported in our previous study [26]. In brief, after anesthetization with intramuscular administration of 3% pentobarbital sodium (30 mg/kg), a cylindrical bone defect (6.0 mm diameter and 8.0 mm length) was created in the lateral condyle of the left femur with an electrical drill. After washing with sterile saline and hydrogen peroxide, the drill-hole defect was filled with a cylindrical block of pTi of a matching size. One day post surgery, an X-ray imaging system (Carestream Health DRX-1, Rochester, NY) was employed to scan the animals to confirm the accuracy of the defect location and implant orientation. One week post surgery, rabbits in the PEMF group were subjected to 2 h/day PEMF stimulation. All rabbits were given two intramuscular injections of 8 mg/kg calcein (Sigma-Aldrich, St. Louis, MO) 11 and 4 days prior to euthanasia. After PEMF treatment for 4 consecutive weeks, all animals were sacrificed by pentobarbital overdose, and blood samples were immediately obtained by cardiac puncture and centrifuged at 5000 rpm to collect serum. The heart, liver, spleen, lung, kidney and brain tissues were immediately harvested and weighed. The left femoral condylar samples were harvested on ice and immersed in 80% ethanol for bone histological and histomorphometric evaluations. The left femoral bone with 2 cm height proximal to the defect site was spun at 5000 rpm for 3 min followed by repeated PBS flushing to remove bone marrow and then snap-frozen in liquid nitrogen for real-time PCR assays. The right femora were frozen in saline-soaked gauze at −70 °C for micro-CT scanning. The right proximal tibiae were fixed in 4% paraformaldehyde (PFA) for osteocyte morphology and survival analyses. All animal care and handling procedures were approved by the Institutional Animal Care and Use Committee of the Fourth Military Medical University.

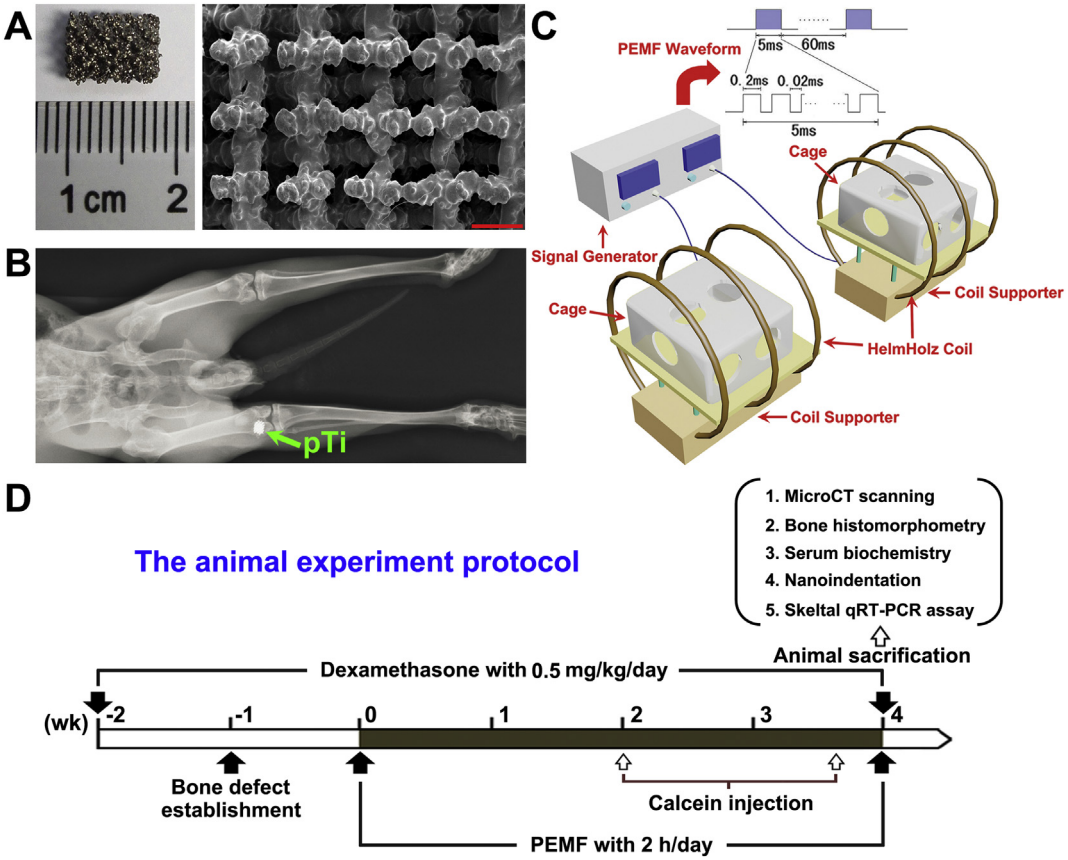

Fig. 1. The porous titanium alloy (pTi) implant, pulsed electromagnetic fields (PEMF) exposure system, and overall experimental protocol used in the current study. (A) Characterization of the Ti2448 pTi implant (6.0 mm diameter, 8.0 mm length, 70% porosity and 750 μm pore size) *via* gross view and scanning electron microscope (SEM) imaging. The scale bar in the SEM image represents 1 mm. (B) X-ray imaging of the rabbit in which a cylindrical bone defect 6.0 mm in diameter and 8.0 mm in length was established in the femoral lateral condyle, and then the pTi implant was transplanted into the bone defect site. (C) The PEMF waveform employed in this study consisted of a pulsed burst (burst width, 5 ms; pulse width, 0.2 ms; pulse wait, 0.02 ms; burst wait, 60 ms; pulse rise, 0.3 μs; pulse fall, 2.0 μs) repeated at 15 Hz. The peak magnetic field intensity within the Helmholtz coils was approximately 2.0 mT. (D) The flow diagram for the experimental protocol used in the current study.

2.3. PEMF exposure system

As described in our previous studies [26,41], a custom-designed PEMF exposure system comprising a signal generator and a Helmholtz coil assembly with a three-coil array was employed (Fig. 1). The three coils were placed coaxially 30.4 cm apart from each other. The turn numbers of the central coil and outside coils were 266 and 500, respectively. It has been proven that this assembly of three coils can produce much higher magnetic field uniformity than the traditional two-coil model [41]. The PEMF output waveform from the signal generator consisted of a pulsed burst (burst width, 5 ms; pulse width, 0.2 ms; pulse wait, 0.02 ms; burst wait, 60 ms; pulse rise, 0.3 μs; pulse fall, 2.0 μs) repeated at 15 Hz (Fig. 1). The peak intensity of the output magnetic fields was approximately 2.0 mT, which was determined using a Gaussmeter (Lake Shore Cryotronics, Westerville, OH). These specific PEMF parameters, including the waveform, intensity and frequency, have proven to be effective at resisting bone loss induced by ovariectomy or diabetes in our previous animal studies [26,41].

2.4. Serum biochemical analysis

Serum biochemical indices, including alanine aminotransferase (ALT), aspartate aminotransferase (AST), total bilirubin (Tbil), total protein (TP), albumin (ALB), creatinine (CRE), glucose (GLU), triglyceride (TG), cholesterol (GHOL), high-density lipoprotein (HDL), and low-density lipoprotein (LDL), were quantified using an automatic analyzer (COBAS INTEGRA 400 plus, Roche, Basel, Switzerland). The commercial enzyme-linked immunosorbent assay (ELISA) kits (CUSABIO Biotech Co., Wuhan, China) were used to determine bone turnover markers, including serum osteocalcin (Cat. No. CSB-E14060Rb), N-terminal propeptide of type 1 procollagen (P1NP, Cat. No. CSB-E17085Rb), tartrate-resistant acid phosphatase 5b (TRACP5b, Cat. No. CSB-E15043Rb), and C-terminal cross-linked telopeptides of type 1 collagen (CTX-1, Cat. No. CSB-E07005Rb). All procedures were strictly performed according to the protocols provided by the manufacturers. The absorbance values of samples were measured at 450 nm (with the correction wavelength at 570 nm) using an Epoch microplate spectrophotometer (Biotek, Winooski, VT).

2.5. Micro-CT imaging

The right femora were assessed by a micro-CT scanning system (Y. Cheetah, YXLON, Germany) with the X-ray source set at 80 kV and 50 μA. Three-dimensional images were reconstructed to 18-μm isotropic voxel size. Based on the VG Studio Max 2.2 software, the trabecular volume of interest (VOI) starting at a distance of 2.5 mm distal from the proximal end plane of the growth plate of the distal femur and extending to the diaphysis over a distance of 5.0 mm was selected, which only contained the second spongiosa. The corresponding characteristic parameters of trabecular bone, including trabecular bone mineral density (BMD), bone volume/total volume (BV/TV), connectivity density (Conn.D), structure model index (SMI), trabecular number (Tb.N), trabecular thickness (Tb.Th), trabecular separation (Tb.Sp) and bone surface per bone volume (BS/BV) were analyzed. The

cortical VOI was selected starting at a position 5.0 mm proximal to the proximal end plane of the trabecular VOI and extending 2.0 mm to the diaphysis, and the cortical thickness (Ct.Th) and cortical area (Ct.Ar) were calculated.

2.6. Histology and histomorphometry

The left femoral condyles were dehydrated progressively in ethanol (from 70% to 100%), embedded in methyl methacrylate, and longitudinally sectioned along the pTi using a Leica 2500E diamond saw microtome (Leica SpA, Milan, Italy) to a thickness of ~50 μm. The mineral apposition rate (MAR, mean distance between the double fluorescent labels divided by the labeling intervals of 7 days) and bone formation rate/bone surface (BFR/BS, double-labeled perimeter plus half of single-labeled perimeter multiplied by MAR per bone surface) were measured in the regions of peri-implant bone and cancellous bone (without bone defect) under a fluorescence microscope (LEICA DM LA, Leica Microsystems, Heidelberg, Germany). After fluorescent imaging, all sections were stained with Masson-Goldner trichrome to further evaluate the trabecular bone architecture and bone ingrowth in pTi, and the bone area fraction was calculated from the pixels representing bone tissue (bone area per total area) in the histological images.

2.7. Osteocyte survival analysis

After fixation in 4% PFA for 2 days, the right proximal tibiae were immersed in 10% EDTA for 8 weeks, and then embedded in paraffin. Five-micron-thick sections were stained with hematoxylin and eosin (H &E) to evaluate the morphology of osteocytes and their lacunae. The number of empty lacunae per trabecular bone surface was analyzed based on the H&E staining images. TUNEL immunofluorescence staining was also performed using a commercial TUNEL staining kit (Roche, Mannheim, FRG) to assess osteocyte apoptosis. The percentage of TUNEL-positive (apoptotic) osteocytes in the trabecular bone matrix was quantified under the Leica fluorescence microscope.

2.8. Nanoindentation tests

The left femoral condyles embedded in methyl methacrylate were longitudinally sectioned along the pTi to ~1 mm thickness and then polished using silicon carbide abrasive paper (grit sizes of 800, 1000 and 1200) under water irrigation. The samples were stored at −20 °C prior to mechanical testing to minimize any changes in material properties [42]. Before testing, the samples were rehydrated in saline for 24 h and then transferred to an Agilent G200 NanoIndenter (Agilent Technologies, Inc., Chandler, AZ) equipped with a Berkovich pyramidal-shaped diamond tip. The load-controlled nanoindentation assays were conducted according to a previously reported protocol [43]. First, the indenter tip was pressed into the specimens to a 4-μm maximum depth with a 0.05 s^{-1} strain rate. The peak load was held for 10 s to minimize the viscoelasticity and creep of skeletal tissues. Then, unloading was applied to 10% of the peak load at the maximum loading rate followed by a 60-s hold for calculating the thermal drift. Following the removal of the tip from the specimen, the modulus and contact hardness were calculated based on the automatically collected force-displacement data using the standard Oliver-Pharr method [44].

2.9. Real-time PCR assays

Prior to RNA extraction, bone specimens were ground to powder in a mortar filled with liquid nitrogen using a pestle. TRIzol was then directly added to the bone powder, and total RNA was isolated using the guanidinium isothiocyanate-phenol-chloroform extraction method following the manufacturer's instructions. Then, cDNA was synthesized from RNA using SuperScript III reverse transcriptase. Quantitative real-time PCR was performed on an ABI PRISM 7300 real-time PCR system using SYBR Green PCR Master Mix (Applied Biosystems, Foster City, CA). The primers were designed (using the Primer-BLAST tool available from the NCBI website) and synthesized by Beijing AuGCT DNA-SYN Biotechnology Co., Ltd. The primers used in the current study are shown in Table S1. The mRNA levels of each gene were normalized to the β-actin mRNA level. The expression levels of genes were calculated using the $2^{-\Delta\Delta Ct}$ method.

2.10. Statistical analysis

Data analyses were performed with SPSS 20.0 for Windows software (Chicago, IL), and expressed as mean ± standard deviation (SD). Based on the normal distribution examination using the Kolmogorov-Smirnov test and homogeneity of variance evaluation using Levene's test, we observed that each specific parameter in the three groups obeyed a normal distribution and homoscedasticity. Then, all experimental data were statistically analyzed using the One-way analysis of variance (ANOVA) with Bonferroni's *post hoc* comparisons. A P value of < 0.05 was considered statistically significant.

3. Results

3.1. Safety evaluation

The effects of PEMF on the organ weights and serum biochemical parameters in GC-treated rabbits are shown in Fig. S1 and Table S2, respectively. Our findings demonstrate that PEMF did not induce any change in either absolute weights or relative weights (normalized by body weights) of various organs in GC-treated rabbits, including the heart, liver, spleen, lung, kidney and brain (Fig. S1, $P > 0.05$). Moreover, PEMF exposure did not cause any change in serum biochemical indices in GC-treated rabbits, including alanine aminotransferase, aspartate aminotransferase, total bilirubin, total protein, albumin, creatinine, glucose, triglyceride, cholesterol, high-density lipoprotein, and low-density lipoprotein (Table S2, $P > 0.05$). Thus, our findings reveal that PEMF did not induce any significant side effects in GC-treated rabbits.

3.2. Micro-CT analysis

Representative micro-CT images of femoral cancellous bone and cortical bone are shown in Fig. 2A & B, respectively. The GC group exhibited deterioration in femoral cancellous bone architecture, as evidenced by the significantly lower trabecular BMD, BV/TV, Conn.D, Tb.N, and Tb.Th ($P < 0.01$) and higher SMI, Tb.Sp and BS/BV ($P < 0.01$) than the Control group (Fig. 2C~J). The PEMF group showed a significant increase in trabecular BMD (+32.1%, $P = 0.004$), BV/TV (+68.3%, $P = 0.004$), Conn.D (+28.2%, $P = 0.003$), and Tb.N (+32.0%, $P = 0.02$), and a decrease in SMI (−18.8%, $P = 0.001$), Tb.Sp (−22.9%, $P = 0.003$) and BS/BV (−19.8%, $P = 0.001$) compared with the GC group (Fig. 2C~J). The PEMF group showed significantly lower BMD and Conn.D, and higher BS/BV than the Control group ($P < 0.05$), whereas no significant difference in BV/TV, SMI, Tb.N, Tb.Th, or Tb.Sp was observed between the PEMF group and the Control group ($P > 0.05$). Moreover, the GC group also showed a significant decrease in cortical bone parameters compared with the Control group, including Ct.Th and Ct.Ar (Fig. 2K & L, $P < 0.01$). The PEMF group also exhibited significant improvement in cortical bone microstructure compared with the GC group, as evidenced by increased Ct.Th (+19.2%, $P = 0.001$) and Ct.Ar (+28.2%, $P = 0.003$).

3.3. Bone histological analysis

Representative femoral cancellous bone histology images in the region of bone defects and in the region without bone defects are shown in Fig. 3A & B, respectively. The GC group exhibited fewer bone

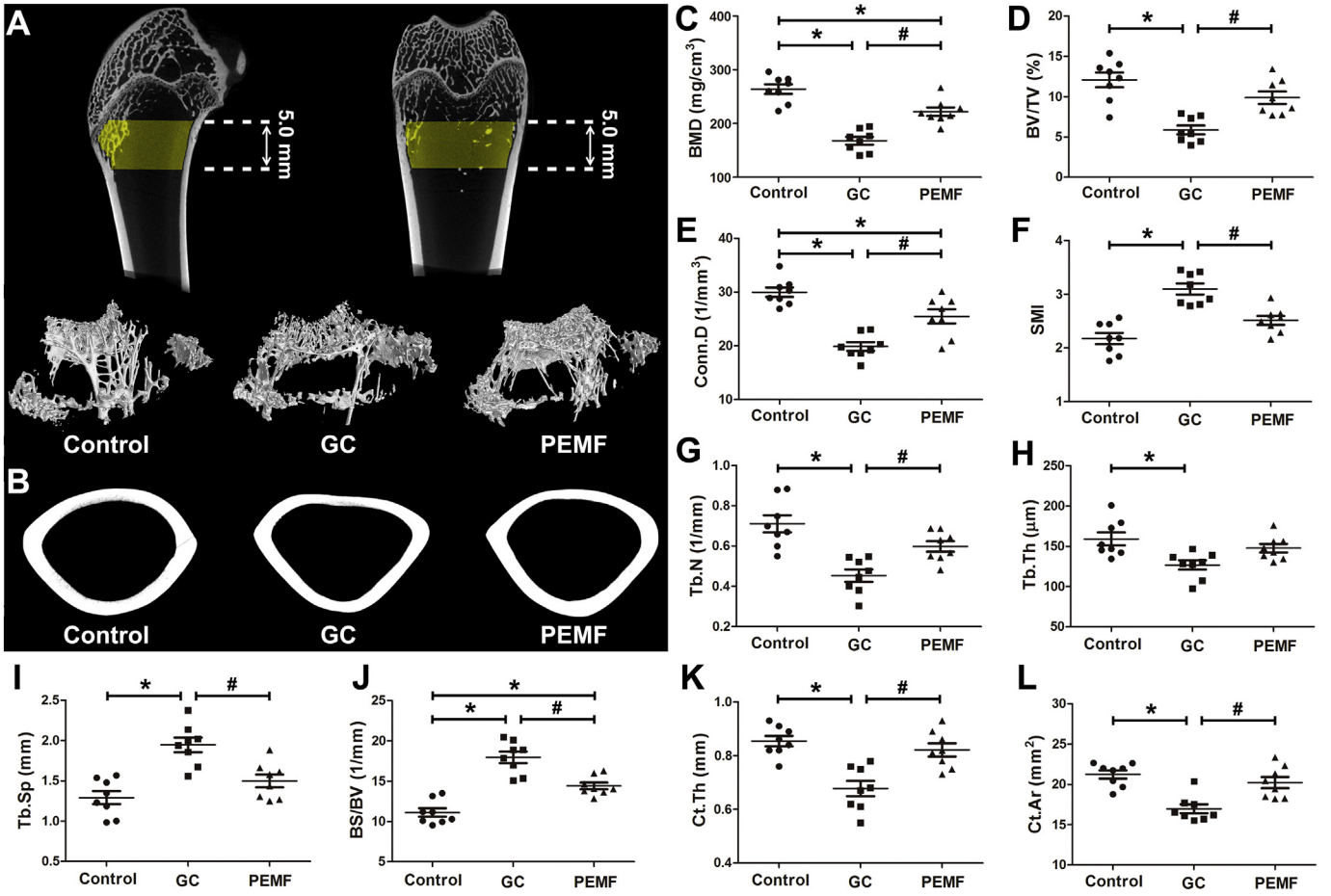

Fig. 2. Effects of pulsed electromagnetic fields (PEMF) exposure on cancellous and cortical bone architecture in distal femora in glucocorticoid-treated rabbits *via* micro-CT imaging. (A) Three-dimensional micro-CT images of cancellous bone architecture of distal femora determined by the selected volume of interest (VOI) with yellow color, which started at a distance of 2.5 mm distal from the proximal end plane of the growth plate and extended to the diaphysis over a distance of 5.0 mm. (B) Two-dimensional femoral cortical bone micro-CT images at the plane that was 5.0 mm proximal to the proximal end plane of the trabecular VOI. (C–J) Statistical analyses for the characteristic parameters of trabecular bone, including trabecular bone mineral density (BMD), bone volume/total volume (BV/TV), connectivity density (Conn.D), structure model index (SMI), trabecular number (Tb.N), trabecular thickness (Tb.Th), trabecular separation (Tb.Sp) and bone surface per bone volume (BS/BV). (K&L) Statistical analyses for the characteristic parameters of cortical bone, including cortical thickness (Ct.Th) and cortical area (Ct.Ar). Control, the blank control rabbits group; GC, the glucocorticoid-treated rabbits group; PEMF, the glucocorticoid-treated rabbits with PEMF exposure group. All data are expressed as mean ± S.D. (n = 8). $^{*}P < 0.05$ *vs.* the Control group; $^{\#}P < 0.05$ *vs.* the GC group. (For interpretation of the references to color in this figure legend, the reader is referred to the web version of this article.)

ingrowths through the pores of Ti2448 pTi implants than the Control group, as evidenced by significantly lower peri-implant bone area fraction (Fig. 3C, $P < 0.001$). The GC-treated rabbits also exhibited deterioration of the cancellous bone microstructure in the region without bone defects, as evidenced by a significantly lower cancellous bone area fraction than the Control group (Fig. 3D, $P < 0.001$). PEMF significantly increased the bone area fraction of peri-implant bone (+251.7%, $P < 0.001$) and cancellous bone (+68.8%, $P = 0.002$) in GC-treated rabbits. However, no significant difference in the bone area fraction of peri-implant bone or cancellous bone was found between the PEMF group and the Control group ($P > 0.05$).

3.4. Nanoindentation testing

The results of the femoral biomechanical material properties *via* nanoindentation testing are shown in Fig. 4. The rabbits in the GC group showed a significantly lower elastic modulus and hardness in both peri-implant trabecular bone and cortical bone than those in the Control group ($P < 0.05$). The PEMF group exhibited significant improvement in the elastic modulus (+29.9%, $P = 0.002$) and hardness (+22.0%, $P = 0.002$) in peri-implant trabecular bone compared with GC-treated rabbits. Moreover, PEMF exposure also significantly increased the cortical bone modulus (+22.9%, $P = 0.009$) and hardness (+28.7%, $P < 0.001$) in GC-treated rabbits. The PEMF group showed lower peri-implant trabecular bone hardness than the Control group ($P < 0.05$), whereas no significant difference in peri-implant trabecular bone modulus or cortical bone modulus/hardness was observed between the PEMF group and Control group ($P > 0.05$).

3.5. Bone turnover examination

Dynamic histomorphometric results based on calcein double labeling showed that GC led to a significant reduction in the peri-implant bone formation rate in the region of bone defects, as evidenced by the greatly decreased MAR and BFR/BS (Fig. 5A, $P < 0.001$). PEMF exposure significantly increased the peri-implant bone MAR (+66.4%, $P < 0.001$) and BFR/BS (+126.4%, $P < 0.001$) levels in GC-treated rabbits. Moreover, the GC group showed significantly lower cancellous bone MAR and BFR/BS than the Control group (Fig. 5B, $P < 0.001$). However, the PEMF group exhibited a significant increase in trabecular bone MAR (+46.3%, $P = 0.018$) and BFR/BS (+114.9%, $P < 0.001$) in comparison with the GC group. Moreover, the serum ELISA results

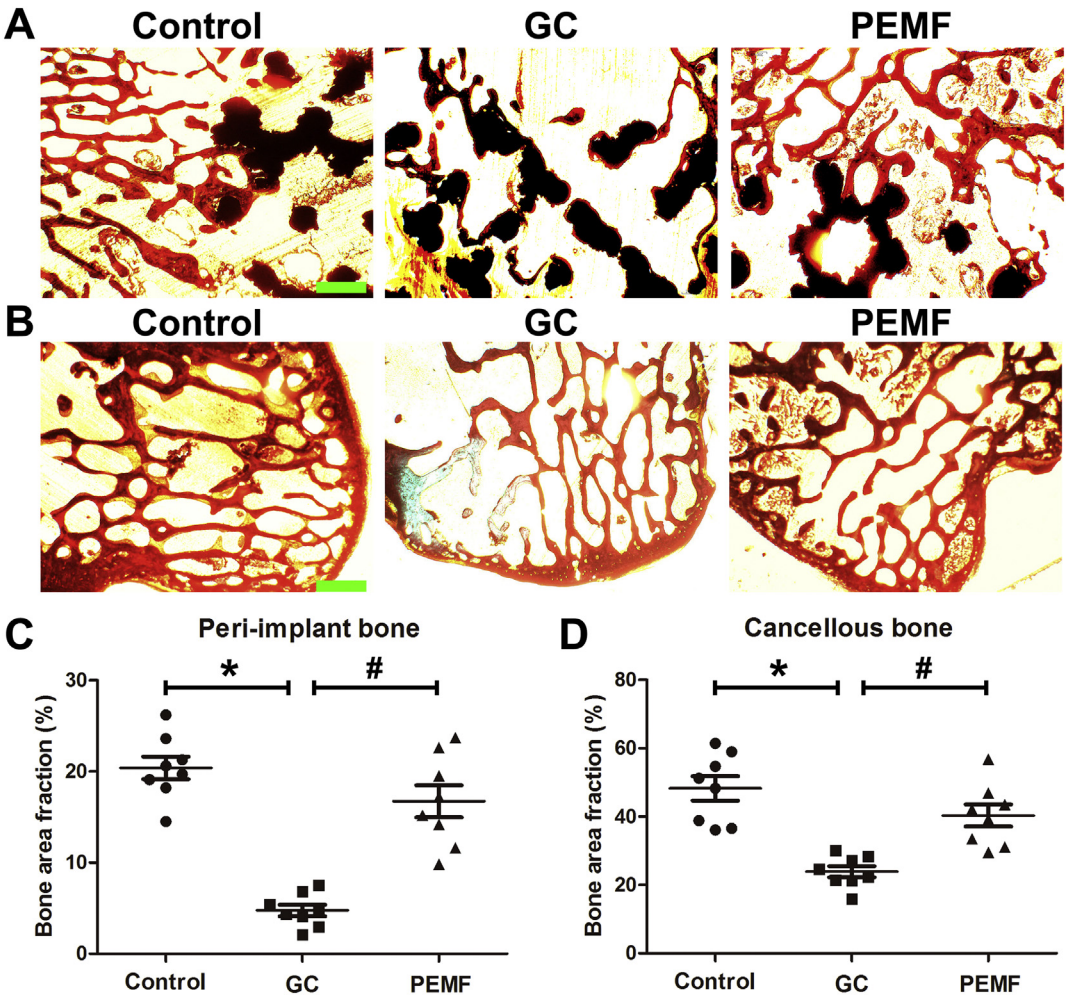

Fig. 3. Effects of pulsed electromagnetic fields (PEMF) stimulation on femoral trabecular bone histology (A) in the region of bone defects and (B) in the region without bone defects in glucocorticoid-treated rabbits *via* Masson-Goldner trichrome staining. The black areas in (A) represent porous titanium (pTi) alloy. Scale bars in (A & B) represent 200 μm. (C & D) The corresponding statistical results of the bone area fraction (bone area per total area) of peri-implant bone and cancellous bone (without bone defect) based on the Masson-Goldner trichrome staining images. Control, the blank control rabbits group; GC, the glucocorticoid-treated rabbits group; PEMF, the glucocorticoid-treated rabbits with PEMF exposure group. All data are expressed as mean ± S.D. (n = 8). $^{*}P < 0.05$ *vs.* the Control group; $^{\#}P < 0.05$ *vs.* the GC group.

demonstrated that the concentrations of bone formation markers, including serum osteocalcin and P1NP, were significantly lower in the GC group than those in the Control group (Fig. 5C & D, $P < 0.001$). The PEMF group exhibited significantly higher serum osteocalcin (+39.6%, $P = 0.008$) and P1NP (+40.7%, $P = 0.001$) concentrations than those in the GC group. No significant difference in MAR, BFR/BS, serum osteocalcin or serum P1NP was observed between the PEMF group and the Control group ($P > 0.05$). We also found that the GC group and the PEMF group exhibited significantly higher serum TRAcP5b and CTX-1 concentrations (Fig. 5E & F, bone resorption markers, $P < 0.01$) than the Control group. Nevertheless, no significant difference was observed in serum TRAcP5b or CTX-1 levels between the GC and PEMF groups ($P > 0.05$).

3.6. Osteocyte survival analysis

Representative osteocyte H&E staining and TUNEL immunofluorescence staining images are depicted in Fig. 6A & B. The H&E staining results demonstrated that the GC group exhibited a significant increase in the numbers of empty lacunae compared with the Control group (Fig. 6A & C, $P < 0.001$). However, in comparison with the GC group, the PEMF group showed a significant decrease in the numbers of empty lacunae (−44.2%, $P < 0.001$). The TUNEL immunofluorescence staining results showed that the GC group had a significantly higher percentage of TUNEL-positive osteocytes than the Control group (Fig. 6B & D, $P < 0.001$). The PEMF group exhibited a significant decrease in the percentage of TUNEL-positive osteocytes compared with the GC group (−52.4%, $P < 0.001$). The PEMF group also showed a significantly lower number of empty lacunae and percentage of TUNEL-positive osteocytes than the Control group ($P < 0.01$).

3.7. Real-time PCR assays

The rabbits in the GC group showed a significant decrease in osteoblast-related gene expression compared with those in the Control group, including osteocalcin, Runx2 and Osx (Fig. 7A–C, $P < 0.001$). The GC and PEMF groups exhibited significantly higher osteoclast-specific gene expression than the Control group, including TRAP and cathepsin K (Fig. 7D & E, $P < 0.001$). PEMF significantly upregulated osteoblast-related osteocalcin, Runx2 and Osx expression ($P < 0.001$) in GC-treated rabbits but had no measurable impact on osteoclast-related TRAP and cathepsin K gene expression ($P > 0.05$). Moreover, PEMF partially attenuated the increase in osteocyte-specific Sost and DKK1 gene expression (Fig. 7F & G, $P < 0.001$), whereas the Sost and DKK1 expression levels in the PEMF group were still lower than those in

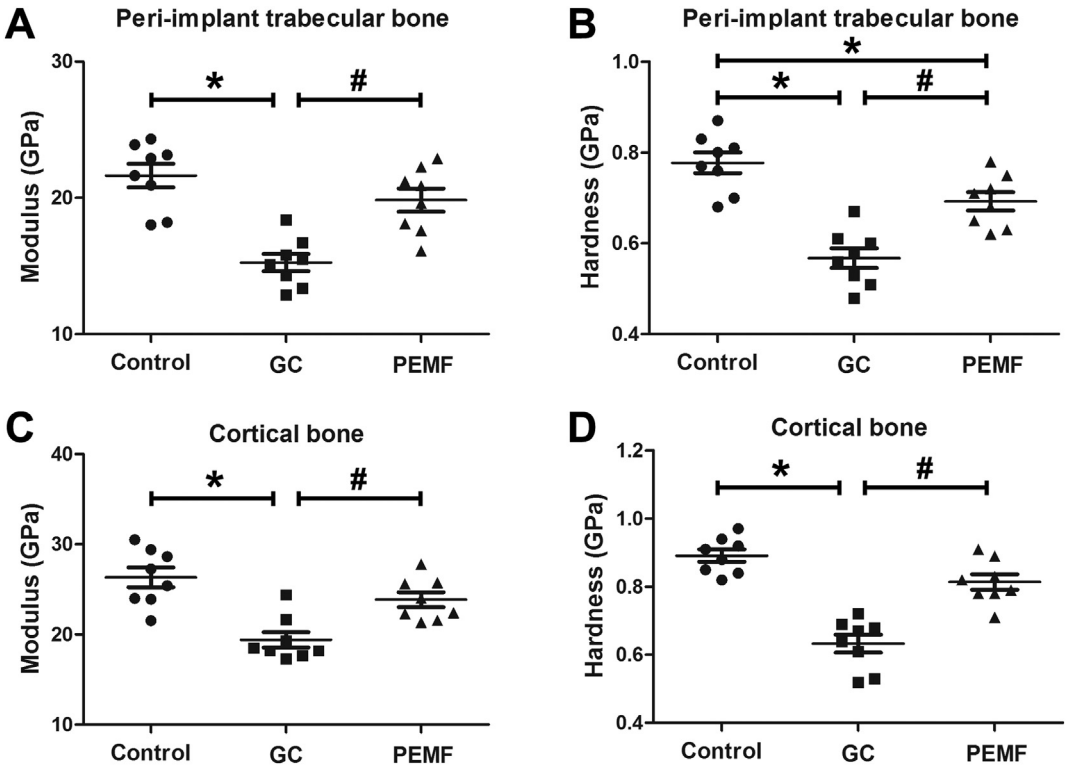

Fig. 4. Effects of pulsed electromagnetic fields (PEMF) exposure on the biomechanical material properties (modulus and hardness) of femoral (A & B) peri-implant trabecular bone and (C & D) cortical bone in glucocorticoid-treated rabbits based on nanoindentation testing. Control, the blank control rabbits group; GC, the glucocorticoid-treated rabbits group; PEMF, the glucocorticoid-treated rabbits with PEMF exposure group. All data are expressed as mean ± S.D. (n = 8). $^{*}P < 0.05$ *vs.* the Control group; $^{\#}P < 0.05$ *vs.* the GC group.

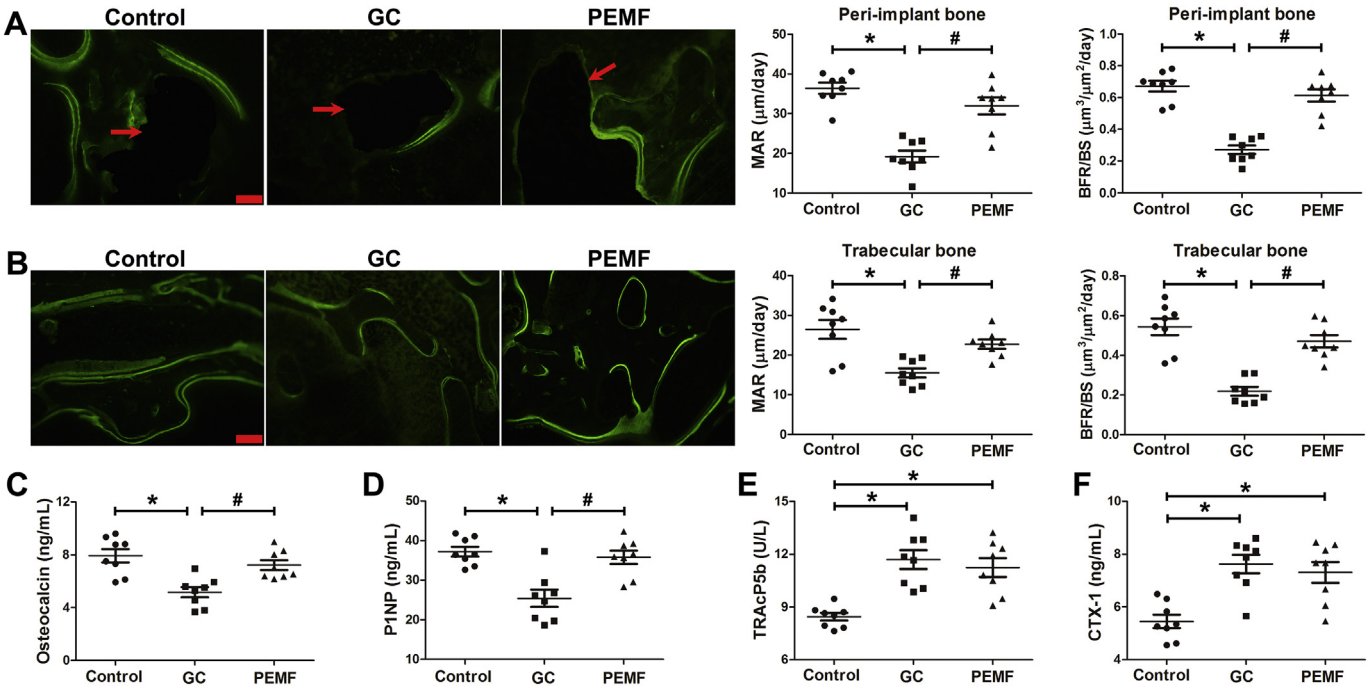

Fig. 5. Effects of pulsed electromagnetic fields (PEMF) stimulation on bone formation and resorption in glucocorticoid-treated rabbits. (A & B) Dynamic histomorphometric analysis of rabbit femoral (A) peri-implant bone and (B) cancellous bone based on dual calcein labeling with 7-day intervals, and the mineral apposition rate (MAR) and bone formation rate per bone surface (BFR/BS) were determined. The black areas in (A) labeled with red arrows represent porous titanium (pTi) alloy. Scale bars in (A&B) represent 200 μm. (C–F) Enzyme-linked immunosorbent assays (ELISA) for the bone formation markers serum osteocalcin and N-terminal propeptide of type 1 procollagen (P1NP), and the bone resorption markers serum tartrate-resistant acid phosphatase 5b (TRAcP5b) and C-terminal cross-linked telopeptides of type 1 collagen (CTX-1). Control, the blank control rabbits group; GC, the glucocorticoid-treated rabbits group; PEMF, the glucocorticoid-treated rabbits with PEMF exposure group. All data are expressed as mean ± S.D. (n = 8). $^{*}P < 0.05$ *vs.* the Control group; $^{\#}P < 0.05$ *vs.* the GC group. (For interpretation of the references to color in this figure legend, the reader is referred to the web version of this article.)

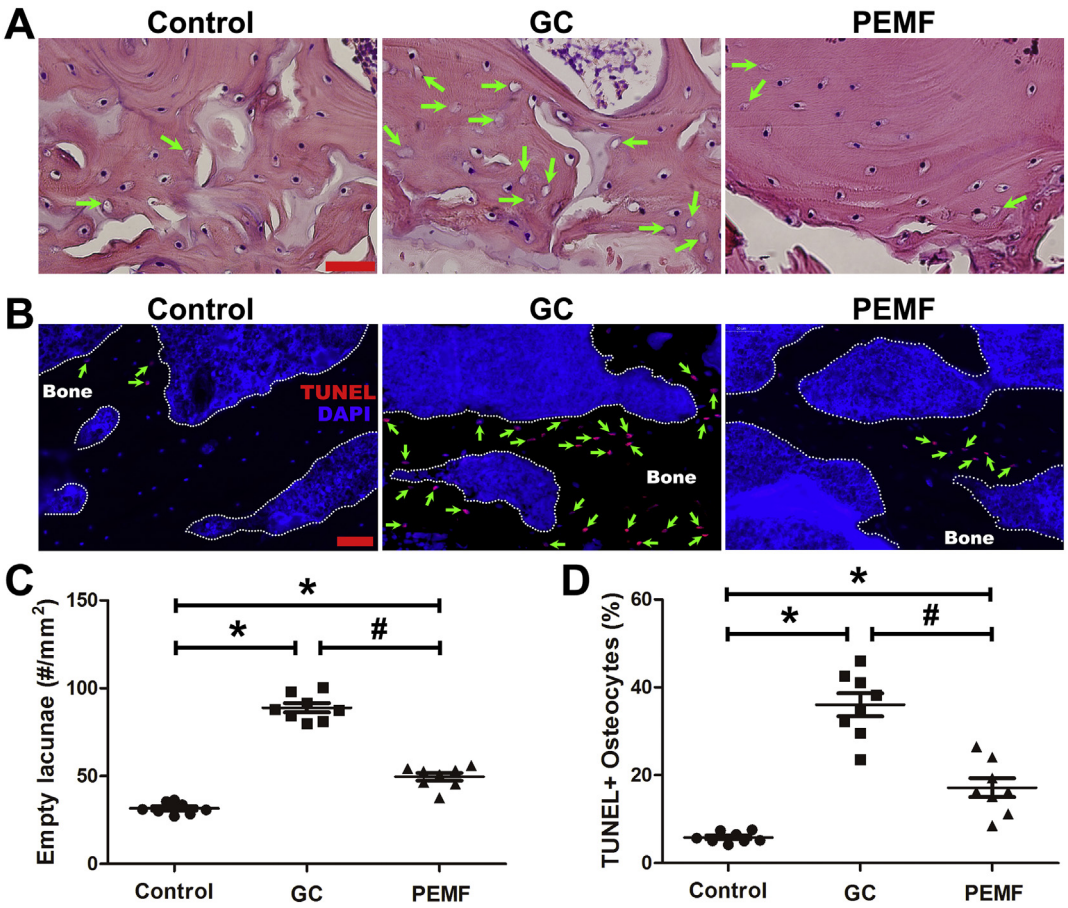

Fig. 6. Effects of pulsed electromagnetic fields (PEMF) exposure on osteocyte survival in glucocorticoid-treated rabbits. (A) Hematoxylin and eosin (H&E) staining on decalcified proximal tibial specimens to visualize the morphology of osteocytes and their lacunae. Empty lacunae are labeled with green arrows. The scale bar represents 100 μm. (B) TUNEL immunofluorescence staining for the apoptotic analysis of osteocytes in decalcified proximal tibial specimens. Apoptotic osteocytes are labeled with green arrows. (C) Statistical results for the parameter of empty lacunae per trabecular bone surface based on the H&E staining images. (D) Statistical results for TUNEL + osteocytes in trabecular bone based on the TUNEL immunofluorescence staining images. Control, the blank control rabbits group; GC, the glucocorticoid-treated rabbits group; PEMF, the glucocorticoid-treated rabbits with PEMF exposure group. All data are expressed as mean ± S.D. (n = 8). $^{*}P < 0.05$ *vs.* the Control group; $^{\#}P < 0.05$ *vs.* the GC group. (For interpretation of the references to color in this figure legend, the reader is referred to the web version of this article.)

the Control group ($P < 0.01$). The GC group also showed a significant decrease in skeletal gene expression of canonical Wnt ligands (Wnt1, Wnt3a and Wnt10b) and β-catenin compared with the Control group (Fig. 7H–L, $P < 0.001$). PEMF significantly upregulated skeletal Wnt1 ($P < 0.001$), Wnt3a ($P < 0.001$), Wnt10b ($P = 0.003$), and β-catenin ($P < 0.001$) gene expression in GC-treated rabbits. However, no detectable difference in non-canonical Wnt5a expression was observed between the GC and PEMF groups (Fig. 7J, $P > 0.05$).

4. Discussion

GC-induced osteoporosis is the second most common form of osteoporosis after postmenopausal osteoporosis [45]. Moreover, bone defect repair in GC-treated osteoporotic skeletons remains a challenging clinical issue for orthopedic surgeons. Considering the dosing inconvenience, side effects, and cost of pharmacotherapy, investigators have endeavored to explore the biophysical treatments for GC-related bone deficits. Studies have shown that resistance exercise and mechanical vibration were able to partially inhibit the deleterious consequences of GC on bone mass [46–48]. Although strong evidence has revealed the positive skeletal effects of low-intensity pulsed ultrasound (LIPUS), LIPUS did not show significant effects on BMD or cancellous bone healing in GC-treated rats [49]. A study by Bayat et al. showed that low-level laser therapy improved the biomechanical properties in GC-induced osteopenic rats [50]. We herein found that PEMF improved cancellous and cortical bone mass, bone quality, and bone defect regeneration in GC-exposed rabbits. This study reveals that PEMF treatment, due to its economic, convenient and noninvasive nature, may become a promising strategy for improving bone health in GC-treated individuals.

According to the micro-CT and histological results, we found that dexamethasone was detrimental to cancellous bone microarchitecture and cortical bone thickness in rabbit femora. Several previous studies also revealed similar structural damage to both trabecular and cortical bone induced by dexamethasone in mice, rats and rabbits [40,51,52]. Interestingly, PEMF partially preserved three-dimensional bone architecture in dexamethasone-treated rabbits, characterized by the significantly improved cancellous bone number and connectivity and increased cortical bone thickness. In addition, we also used the biomechanical nanoindentation technique to determine the modification of bone's intrinsic material quality at the microscale. The major characteristic parameters of skeletal material properties, including modulus and hardness, were markedly reduced in the presence of dexamethasone. Similarly, Balooch et al. also found a GC-induced decline in biomechanical material properties in mouse and human trabecular bone based on indentation measurements [53]. Moreover, we also observed that compromised skeletal microscopic mechanical properties were partially reversed by PEMF, as evidenced by the

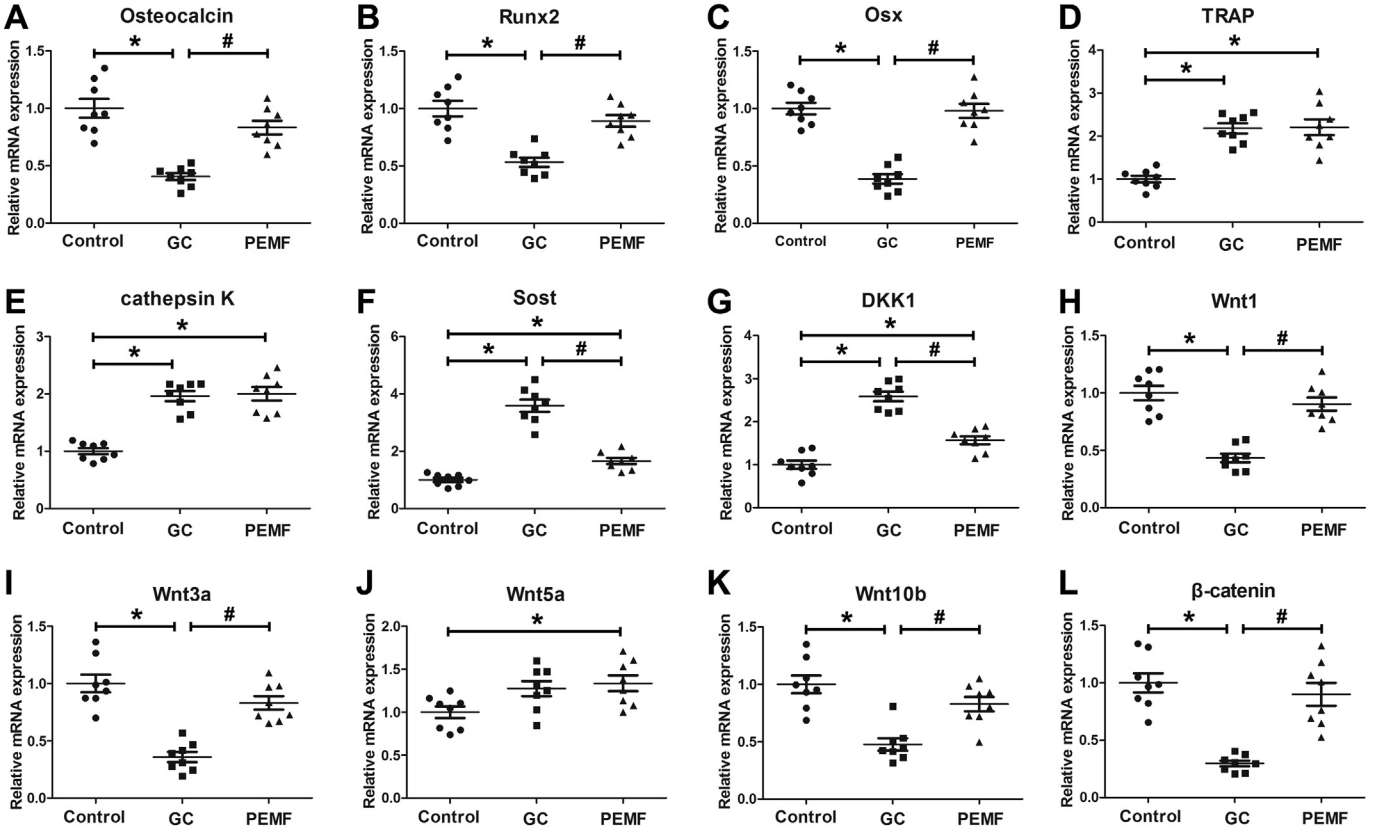

Fig. 7. Effects of pulsed electromagnetic fields (PEMF) exposure on gene expression in femoral bones with 2 cm height above the bone defect site with removal of bone marrow in glucocorticoid-treated rabbits *via* real-time PCR analyses, including (A) Osteocalcin, (B) Runx2, (C) Osx, (D) TRAP, (E) cathepsin K, (F) Sost, (G) DKK1, (H) Wnt1, (I) Wnt3a, (J) Wnt5a, (K) Wnt10b, and (L) β-catenin. Control, the blank control rabbits group; GC, the glucocorticoid-treated rabbits group; PEMF, the glucocorticoid-treated rabbits with PEMF exposure group. All data are expressed as mean ± S.D. (n = 8). $^{*}P < 0.05$ *vs.* the Control group; $^{\#}P < 0.05$ *vs.* the GC group.

increased elastic modulus and hardness. Thus, our findings reveal that PEMF stimulation has the capacity to inhibit GC-induced deteriorations of bone quality in addition to bone mass and microarchitecture.

Our ELISA results demonstrate that circulating osteocalcin and P1NP levels, two critical biomarkers highly correlated with bone formation [54,55], were significantly increased by PEMF exposure in GC-treated rabbits. Consistent with the serum findings, dynamic histomorphometric results provide further direct evidence that the GC-mediated decrease in bone formation rates was significantly attenuated by PEMF treatment. The PCR results demonstrate that PEMF stimulated the gene expression of Runx2 and Osx, two specific transcriptional regulatory factors that are essential for osteoblast differentiation [56]. PEMF exposure was also found to promote skeletal OCN expression in GC-treated rabbits, confirming the improvement in osteoblast differentiation. Thus, based on a combination of evidence from serum biochemistry, bone histomorphometry, and skeletal gene expression analyses, our study confirms the reversal of the adverse effects of GC on skeletal anabolism in the presence of PEMF. Similarly, several other investigators have also revealed the bone anabolic effects induced by exogenous electromagnetic stimulation in normal young rats [57–59]. However, our serum biochemistry and skeletal gene expression findings reveal that PEMF exerted no significant effect on osteoclast activity and bone resorption. A similar finding has also been reported in a previous *in vivo* study [26]. However, the reason why osteoblasts and osteoclasts are so different with respect to detecting and responding to external PEMF signals remains unknown. This interesting and important question needs to be further clarified in future studies.

Growing evidence suggests that osteocytes, the most abundant cell type in the skeleton comprising 90–95% of all bone cells, are essential for regulating bone remodeling and maintaining bone mass [60]. Osteocytes are also highly susceptible to the adverse effects of GC [10]. Our H&E and TUNEL staining results demonstrate that chronic GC therapy increased osteocyte apoptosis and disrupted the lacunar-canalicular structures of osteocytes. After PEMF treatment, the numbers of empty lacunae and apoptotic osteocytes in GC-treated rabbits were significantly decreased, revealing PEMF-mediated improvement in osteocyte survival. Our previous *in vitro* study also shows the beneficial effects of PEMF on the viability and connectivity of osteocyte-like MLO-Y4 cells [61]. Furthermore, the PCR results show that PEMF markedly mitigated the GC-induced increase in the gene expression of DKK1 and Sost, two osteocyte-derived negative regulators of osteoblastic functions. Hence, our results reveal that PEMF-mediated skeletal anabolism in GC-treated conditions is associated with the improvement in the viability and function of the osteocyte network.

It has also been shown that the canonical Wnt signaling pathway in osteoblasts was suppressed by chronic GC exposure both *in vivo* and *in vitro* [32,62]. Consistent with these findings, this study shows that GC inhibited the gene expression of canonical Wnt ligands (including Wnt1, Wnt3a and Wnt10b) and β-catenin, providing further evidence that the canonical Wnt signaling cascade was impaired in the GC-treated skeleton. Interestingly, PEMF treatment was able to stimulate the expression of various canonical Wnt ligands as well as their downstream β-catenin, revealing the potential activation of skeletal canonical Wnt signaling in GC-treated rabbits. However, we found no significant change in non-canonical Wnt5a expression in bone exposed to either GC or PEMF. Therefore, our results demonstrate that the PEMF-induced strong bone anabolism in GC-treated skeletons might be associated with the potential activation of canonical Wnt/β-catenin

signaling.

Considering that patients with chronic GC treatment tend to have delayed fracture union and poor bone defect regeneration [63–65], this study also investigated the effects of PEMF on titanium implant osseointegration in GC-treated rabbits. Due to the lower elastic modulus, the Ti2248 pTi implant has been proven to induce lower stress concentrations at the bone-implant interface, and to thus achieve better osseointegration and a lower risk of implant loosening than the commercial Ti-6Al-4V alloy [66]. Our histological, histomorphometric and biomechanical results show that PEMF not only stimulated bone ingrowths into the pore spaces of titanium implants in osseous defects but also improved peri-implant bone material properties and the bone formation rate in GC-treated rabbits, which is beneficial for securing the long-term stability of implant fixation. However, how PEMF treatment improves pTi osseointegration is a complicated issue involving a battery of biological events. PEMF may induce both changes in the electric potential gradients on the titanium surface and surface polarization on the cell membrane and thus promote bone cell/tissue adhesion to the titanium surface [67]. In addition, PEMF treatment may also cause a change in the mechanical microenvironment at the bone-implant interface, which is important for bony ingrowth into a porous implant [68]. Furthermore, PEMF may force ion movement, and alter ion/ligand binding and transport in bone cells [24,69]. It has also been suggested that PEMF may induce ion vibration within bone cells, forcing the opening of voltage gated channels, thus altering the downstream biological cascades associated with bone repair and regeneration [24,70]. Therefore, much work remains to be done in future to clarify the mechanisms by which PEMF exposure promotes peri-implant bone growth in normal and osteoporotic individuals.

One major limitation of this study is the lack of an additional group of normal rabbits with PEMF stimulation. Although the positive effects of PEMF treatment on promoting osteogenesis and increasing bone mass in healthy animals have been systematically reported in our and others' previous studies [34,57,58,71], an additional group of normal rabbits with PEMF will be helpful for providing a more direct comparison of PEMF-induced anabolic effects between normal and GC-treated rabbits.

In conclusion, this study shows that low-intensity PEMF treatment was able to partially inhibit the deleterious consequences of GC on the cancellous and cortical bone architecture and mechanical properties in rabbits. Utilizing the Ti2448 pTi implants with low toxicity and low elastic modulus, we also found that PEMF enhanced peri-implant bone quantity and quality in GC-treated rabbits, revealing improved implant osseointegration and potentially decreased risks of implant loosening during osseous defect repair. Furthermore, our results reveal that PEMF exhibited potent bone-anabolic actions by ameliorating the detrimental effects of GC on the functional activities of osteoblasts and osteocytes, which might be associated with the activation of canonical Wnt signaling. This study highlights that PEMF may represent an effective alternative strategy for the treatment of GC-related bone disorders.

Declaration of competing interest

All authors state that they have no conflicts of interest.

Acknowledgements

The authors acknowledge the support from the National Natural Science Foundation of China (Nos. 51907111, 31500760, 11972366 and 31670953), the Shaanxi Provincial Natural Science Foundation of China (No. 2018JQ8056), the Supporting Project of Young Technology Nova of Shaanxi Province (2019KJXX-087) and the Scientific Research Program Funded by Shaanxi Provincial Education Department (19JK0242).

Author contributions

All authors contributed to the manuscript. D.J., X.F. and E.P.L. designed research. J.C., X.S., Q.J.Y., Y.Q.Y. and Z.D.Y. performed research. J.C., D.J., X.S., Z.D.Y. and E.P.L. analyzed data. J.C., D.J. and X.S. wrote the paper. All authors reviewed the manuscript. J.C. and X.S. are co-first authors.

Appendix A. Supplementary data

Supplementary data to this article can be found online at https://doi.org/10.1016/j.bone.2020.115266.

References

[1] P.J. Barnes, I.M. Adcock, Glucocorticoid resistance in inflammatory diseases, Lancet 373 (9678) (2009) 1905–1917.
[2] A.L. Buchman, Side effects of corticosteroid therapy, J. Clin. Gastroenterol. 33 (4) (2001) 289–294.
[3] K.E. Hansen, H.A. Wilson, C. Zapalowski, H.A. Fink, S. Minisola, R.A. Adler, Uncertainties in the prevention and treatment of glucocorticoid-induced osteoporosis, J. Bone Miner. Res. 26 (9) (2011) 1989–1996.
[4] R.S. Weinstein, Glucocorticoid-induced osteoporosis and osteonecrosis, Endocrinol. Metab. Clin. N. Am. 41 (3) (2012) 595–611.
[5] E. Canalis, G. Mazziotti, A. Giustina, J.P. Bilezikian, Glucocorticoid-induced osteoporosis: pathophysiology and therapy, Osteoporos. Int. 18 (10) (2007) 1319–1328.
[6] R.S. Weinstein, Clinical practice. Glucocorticoid-induced bone disease, N. Engl. J. Med. 365 (1) (2011) 62–70.
[7] T.P. van Staa, The pathogenesis, epidemiology and management of glucocorticoid-induced osteoporosis, Calcif. Tissue Int. 79 (3) (2006) 129–137.
[8] J.S. Carvas, R.M. Pereira, V.F. Caparbo, P. Fuller, C.A. Silveira, L.A. Lima, E. Bonfa, S.B. Mello, A single dose of zoledronic acid reverses the deleterious effects of glucocorticoids on titanium implant osseointegration, Osteoporos. Int. 21 (10) (2010) 1723–1729.
[9] M.A. de Oliveira, D.A. Asahi, C.A.E. Silveira, L. Lima, M. Glick, M. Gallottini, The effects of zoledronic acid and dexamethasone on osseointegration of endosseous implants: histological and histomorphometrical evaluation in rats, Clin. Oral Implants Res. 26 (4) (2015) e17–e21.
[10] X. Xia, R. Kar, J. Gluhak-Heinrich, W. Yao, N.E. Lane, L.F. Bonewald, S.K. Biswas, W.K. Lo, J.X. Jiang, Glucocorticoid-induced autophagy in osteocytes, J. Bone Miner. Res. 25 (11) (2010) 2479–2488.
[11] A.Y. Sato, M. Cregor, J. Delgado-Calle, K.W. Condon, M.R. Allen, M. Peacock, L.I. Plotkin, T. Bellido, Protection from glucocorticoid-induced osteoporosis by anti-catabolic signaling in the absence of sost/sclerostin, J. Bone Miner. Res. 31 (10) (2016) 1791–1802.
[12] L. Gifre, S. Ruiz-Gaspa, A. Monegal, B. Nomdedeu, X. Filella, N. Guanabens, P. Peris, Effect of glucocorticoid treatment on Wnt signalling antagonists (sclerostin and Dkk-1) and their relationship with bone turnover, Bone 57 (1) (2013) 272–276.
[13] K.G. Saag, J.R. Zanchetta, J.P. Devogelaer, R.A. Adler, R. Eastell, K. See, J.H. Krege, K. Krohn, M.R. Warner, Effects of teriparatide versus alendronate for treating glucocorticoid-induced osteoporosis: thirty-six-month results of a randomized, double-blind, controlled trial, Arthritis Rheum. 60 (11) (2009) 3346–3355.
[14] S.H. Yoon, M. Grynpas, J. Mitchell, Intermittent PTH treatment improves bone and muscle in glucocorticoid treated Mdx mice: a model of Duchenne Muscular Dystrophy, Bone 121 (2019) 232–242.
[15] L.F. de Castro, D. Lozano, S. Dapia, S. Portal-Nunez, J.R. Caeiro, E. Gomez-Barrena, P. Esbrit, Role of the N- and C-terminal fragments of parathyroid-hormone-related protein as putative therapies to improve bone regeneration under high glucocorticoid treatment, Tissue Eng Part A 16 (4) (2010) 1157–1168.
[16] W. Yao, W. Dai, L. Jiang, E.Y. Lay, Z. Zhong, R.O. Ritchie, X. Li, H. Ke, N.E. Lane, Sclerostin-antibody treatment of glucocorticoid-induced osteoporosis maintained bone mass and strength, Osteoporos. Int. 27 (1) (2016) 283–294.
[17] Z. Achiou, H. Toumi, J. Touvier, A. Boudenot, R. Uzbekov, M.S. Ominsky, S. Pallu, E. Lespessailles, Sclerostin antibody and interval treadmill training effects in a rodent model of glucocorticoid-induced osteopenia, Bone 81 (2015) 691–701.
[18] J.H. McElhaney, R. Stalnaker, R. Bullard, Electric fields and bone loss of disuse, J. Biomech. 1 (1) (1968) 47–52.
[19] B.T. O'Connor, H.M. Charlton, J.D. Currey, D.R. Kirby, C. Woods, Effects of electric current on bone in vivo, Nature 222 (5189) (1969) 162–163.
[20] C.A. Bassett, R.J. Pawluk, A.A. Pilla, Augmentation of bone repair by inductively coupled electromagnetic fields, Science 184 (4136) (1974) 575–577.
[21] C.A. Bassett, Beneficial effects of electromagnetic fields, J. Cell. Biochem. 51 (4) (1993) 387–393.
[22] V. Cane, P. Botti, S. Soana, Pulsed magnetic fields improve osteoblast activity during the repair of an experimental osseous defect, J. Orthop. Res. 11 (5) (1993) 664–670.
[23] M.J. Crowe, Z.P. Sun, J.H. Battocletti, M.Y. Macias, F.A. Pintar, D.J. Maiman, Exposure to pulsed magnetic fields enhances motor recovery in cats after spinal cord injury, Spine (Phila Pa 1976) 28 (24) (2003) 2660–2666.
[24] C. Daish, R. Blanchard, K. Fox, P. Pivonka, E. Pirogova, The application of pulsed

electromagnetic fields (PEMFs) for bone fracture repair: past and perspective findings, Ann. Biomed. Eng. 46 (4) (2018) 525–542.
[25] D.H. Trock, A.J. Bollet, R.H. Dyer Jr., L.P. Fielding, W.K. Miner, R. Markoll, A double-blind trial of the clinical effects of pulsed electromagnetic fields in osteoarthritis, J. Rheumatol. 20 (3) (1993) 456–460.
[26] J. Cai, W. Li, T. Sun, X. Li, E. Luo, D. Jing, Pulsed electromagnetic fields preserve bone architecture and mechanical properties and stimulate porous implant osseointegration by promoting bone anabolism in type 1 diabetic rabbits, Osteoporos. Int. 29 (5) (2018) 1177–1191.
[27] K. Chang, W.H. Chang, Pulsed electromagnetic fields prevent osteoporosis in an ovariectomized female rat model: a prostaglandin E2-associated process, Bioelectromagnetics 24 (3) (2003) 189–198.
[28] W.W. Shen, J.H. Zhao, Pulsed electromagnetic fields stimulation affects BMD and local factor production of rats with disuse osteoporosis, Bioelectromagnetics 31 (2) (2010) 113–119.
[29] A. Catalano, S. Loddo, F. Bellone, C. Pecora, A. Lasco, N. Morabito, Pulsed electromagnetic fields modulate bone metabolism via RANKL/OPG and Wnt/beta-catenin pathways in women with postmenopausal osteoporosis: a pilot study, Bone 116 (2018) 42–46.
[30] S. Zhu, H. He, C. Zhang, H. Wang, C. Gao, X. Yu, C. He, Effects of pulsed electromagnetic fields on postmenopausal osteoporosis, Bioelectromagnetics 38 (6) (2017) 406–424.
[31] R. Baron, M. Kneissel, WNT signaling in bone homeostasis and disease: from human mutations to treatments, Nat. Med. 19 (2) (2013) 179–192.
[32] K. Ohnaka, M. Tanabe, H. Kawate, H. Nawata, R. Takayanagi, Glucocorticoid suppresses the canonical Wnt signal in cultured human osteoblasts, Biochem. Biophys. Res. Commun. 329 (1) (2005) 177–181.
[33] C.C. Lin, R.W. Lin, C.W. Chang, G.J. Wang, K.A. Lai, Single-pulsed electromagnetic field therapy increases osteogenic differentiation through Wnt signaling pathway and sclerostin downregulation, Bioelectromagnetics 36 (7) (2015) 494–505.
[34] D. Jing, M. Zhai, S. Tong, F. Xu, J. Cai, G. Shen, Y. Wu, X. Li, K. Xie, J. Liu, Q. Xu, E. Luo, Pulsed electromagnetic fields promote osteogenesis and osseointegration of porous titanium implants in bone defect repair through a Wnt/beta-catenin signaling-associated mechanism, Sci. Rep. 6 (2016) 32045.
[35] J. Zhou, H. He, L. Yang, S. Chen, H. Guo, L. Xia, H. Liu, Y. Qin, C. Liu, X. Wei, Y. Zhou, C. He, Effects of pulsed electromagnetic fields on bone mass and Wnt/beta-catenin signaling pathway in ovariectomized rats, Arch. Med. Res. 43 (4) (2012) 274–282.
[36] E. Piters, E. Boudin, W. Van Hul, Wnt signaling: a win for bone, Arch. Biochem. Biophys. 473 (2) (2008) 112–116.
[37] Y.L. Hao, S.J. Li, S.Y. Sun, C.Y. Zheng, R. Yang, Elastic deformation behaviour of Ti-24Nb-4Zr-7.9Sn for biomedical applications, Acta Biomater. 3 (2) (2007) 277–286.
[38] D. Kuroda, M. Niinomi, M. Morinaga, Y. Kato, T. Yashiro, Design and mechanical properties of new β type titanium alloys for implant materials, Mater. Sci. Eng. A 243 (1) (1998) 244–249.
[39] J. Shi, L. Wang, H. Zhang, Q. Jie, X. Li, Q. Shi, Q. Huang, B. Gao, Y. Han, K. Guo, J. Liu, L. Yang, Z. Luo, Glucocorticoids: dose-related effects on osteoclast formation and function via reactive oxygen species and autophagy, Bone 79 (2015) 222–232.
[40] R.I. Gafni, E.F. McCarthy, T. Hatcher, J.L. Meyers, N. Inoue, C. Reddy, M. Weise, K.M. Barnes, V. Abad, J. Baron, Recovery from osteoporosis through skeletal growth: early bone mass acquisition has little effect on adult bone density, FASEB J. 16 (7) (2002) 736–738.
[41] D. Jing, G. Shen, J. Huang, K. Xie, J. Cai, Q. Xu, X. Wu, E. Luo, Circadian rhythm affects the preventive role of pulsed electromagnetic fields on ovariectomy-induced osteoporosis in rats, Bone 46 (2) (2010) 487–495.
[42] J.P. Callaghan, S.M. McGill, Frozen storage increases the ultimate compressive load of porcine vertebrae, J. Orthop. Res. 13 (5) (1995) 809–812.
[43] G.A. Williams, K.E. Callon, M. Watson, J.L. Costa, Y. Ding, M. Dickinson, Y. Wang, D. Naot, I.R. Reid, J. Cornish, Skeletal phenotype of the leptin receptor-deficient db/db mouse, J. Bone Miner. Res. 26 (8) (2011) 1698–1709.
[44] W.C. Oliver, G.M. Pharr, An improved technique for determining hardness and elastic modulus, J. Mater. Res. 7 (6) (1992) 1564–1583.
[45] N. Maruotti, A. Corrado, F.P. Cantatore, Glucocorticoid induced risk of fractures, Panminerva Med. 52 (4) (2010) 339–343.
[46] M.L. de Oliveira, C.T. Bergamaschi, O.L. Silva, K.O. Nonaka, C.C. Wang, A.B. Carvalho, V. Jorgetti, R.R. Campos, M. Lazaretti-Castro, Mechanical vibration preserves bone structure in rats treated with glucocorticoids, Bone 46 (6) (2010) 1516–1521.
[47] K. Pichler, C. Loreto, R. Leonardi, T. Reuber, A.M. Weinberg, G. Musumeci, RANKL is downregulated in bone cells by physical activity (treadmill and vibration stimulation training) in rat with glucocorticoid-induced osteoporosis, Histol. Histopathol. 28 (9) (2013) 1185–1196.
[48] T. Matsuo, T. Nozaki, K. Okamura, K. Matsumoto, T. Doi, S. Gohtani, M. Suzuki, Effects of voluntary resistance exercise and high-protein snack on bone mass, composition, and strength in rats given glucocorticoid injections, Biosci. Biotechnol. Biochem. 67 (12) (2003) 2518–2523.
[49] T. Kawano, N. Miyakoshi, Y. Kasukawa, M. Hongo, H. Tsuchie, C. Sato, M. Fujii, M. Suzuki, M. Akagawa, Y. Ono, Y. Yuasa, I. Nagahata, Y. Shimada, Effects of combined therapy of alendronate and low-intensity pulsed ultrasound on metaphyseal bone repair after osteotomy in the proximal tibia of glucocorticoid-induced osteopenia rats, Osteoporos Sarcopenia 3 (4) (2017) 185–191.
[50] M. Bayat, M. Fridoni, H. Nejati, A. Mostafavinia, M. Salimi, M. Ghatrehsamani, M.A. Abdollahifar, A. Najar, S. Bayat, F. Rezaei, An evaluation of the effect of pulsed wave low-level laser therapy on the biomechanical properties of the vertebral body in two experimental osteoporosis rat models, Lasers Med. Sci. 31 (2) (2016) 305–314.
[51] M. Marenzana, K. Greenslade, A. Eddleston, R. Okoye, D. Marshall, A. Moore, M.K. Robinson, Sclerostin antibody treatment enhances bone strength but does not prevent growth retardation in young mice treated with dexamethasone, Arthritis Rheum. 63 (8) (2011) 2385–2395.
[52] J.L. Ferretti, O. Gaffuri, R. Capozza, G. Cointry, C. Bozzini, M. Olivera, J.R. Zanchetta, C.E. Bozzini, Dexamethasone effects on mechanical, geometric and densitometric properties of rat femur diaphyses as described by peripheral quantitative computerized tomography and bending tests, Bone 16 (1) (1995) 119–124.
[53] G. Balooch, W. Yao, J.W. Ager, M. Balooch, R.K. Nalla, A.E. Porter, R.O. Ritchie, N.E. Lane, The aminobisphosphonate risedronate preserves localized mineral and material properties of bone in the presence of glucocorticoids, Arthritis Rheum. 56 (11) (2007) 3726–3737.
[54] L.V. Hale, R.J. Galvin, J. Risteli, Y.L. Ma, A.K. Harvey, X. Yang, R.L. Cain, Q. Zeng, C.A. Frolik, M. Sato, A.L. Schmidt, A.G. Geiser, PINP: a serum biomarker of bone formation in the rat, Bone 40 (4) (2007) 1103–1109.
[55] R. Civitelli, R. Armamento-Villareal, N. Napoli, Bone turnover markers: understanding their value in clinical trials and clinical practice, Osteoporos. Int. 20 (6) (2009) 843–851.
[56] K. Nakashima, B. de Crombrugghe, Transcriptional mechanisms in osteoblast differentiation and bone formation, Trends Genet. 19 (8) (2003) 458–466.
[57] Y.Y. Wang, X.Y. Pu, W.G. Shi, Q.Q. Fang, X.R. Chen, H.R. Xi, Y.H. Gao, J. Zhou, C.J. Xian, K.M. Chen, Pulsed electromagnetic fields promote bone formation by activating the sAC-cAMP-PKA-CREB signaling pathway, J. Cell. Physiol. 234 (3) (2019) 2807–2821.
[58] J. Zhou, Y.H. Gao, B.Y. Zhu, J.L. Shao, H.P. Ma, C.J. Xian, K.M. Chen, Sinusoidal electromagnetic fields increase peak bone mass in rats by activating Wnt10b/beta-catenin in primary cilia of osteoblasts, J. Bone Miner. Res. 34 (7) (2019) 1336–1351.
[59] H.M. Bilgin, F. Celik, M. Gem, V. Akpolat, I. Yildiz, A. Ekinci, M.S. Ozerdem, S. Tunik, Effects of local vibration and pulsed electromagnetic field on bone fracture: a comparative study, Bioelectromagnetics 38 (5) (2017) 339–348.
[60] L.F. Bonewald, The amazing osteocyte, J. Bone Miner. Res. 26 (2) (2011) 229–238.
[61] P. Wang, C. Tang, J. Wu, Y. Yang, Z. Yan, X. Liu, X. Shao, M. Zhai, J. Gao, S. Liang, E. Luo, D. Jing, Pulsed electromagnetic fields regulate osteocyte apoptosis, RANKL/OPG expression, and its control of osteoclastogenesis depending on the presence of primary cilia, J. Cell. Physiol. 234 (7) (2019) 10588–10601.
[62] N. Guanabens, L. Gifre, P. Peris, The role of Wnt signaling and sclerostin in the pathogenesis of glucocorticoid-induced osteoporosis, Curr Osteoporos Rep 12 (1) (2014) 90–97.
[63] J. Snall, S. Apajalahti, A.L. Suominen, J. Tornwall, H. Thoren, Influence of perioperative dexamethasone on delayed union in mandibular fractures: a clinical and radiological study, Med. Oral Patol. Oral Cir. Bucal. 20 (5) (2015) e621–e626.
[64] A. Ouanounou, S. Hassanpour, M. Glogauer, The influence of systemic medications on osseointegration of dental implants, J. Can. Dent. Assoc. 82 (2016) g7.
[65] J.H. Fu, J.D. Bashutski, K. Al-Hezaimi, H.L. Wang, Statins, glucocorticoids, and nonsteroidal anti-inflammatory drugs: their influence on implant healing, Implant. Dent. 21 (5) (2012) 362–367.
[66] K. Zheng, X. Li, J. Fu, X. Fan, P. Wang, Y. Hao, S. Li, H. Fan, Z. Guo, Effects of Ti2448 half-pin with low elastic modulus on pin loosening in unilateral external fixation, J Mater Sci Mater Med 22 (6) (2011) 1579–1588.
[67] J. Wang, Y. An, F. Li, D. Li, D. Jing, T. Guo, E. Luo, C. Ma, The effects of pulsed electromagnetic field on the functions of osteoblasts on implant surfaces with different topographies, Acta Biomater. 10 (2) (2014) 975–985.
[68] Y.X. Qin, K.J. McLeod, F. Guilak, F.P. Chiang, C.T. Rubin, Correlation of bony ingrowth to the distribution of stress and strain parameters surrounding a porous-coated implant, J. Orthop. Res. 14 (6) (1996) 862–870.
[69] M.S. Markov, Pulsed electromagnetic field therapy history, state of the art and future, Environmentalist 27 (4) (2007) 465–475.
[70] D.J. Panagopoulos, A. Karabarbounis, L.H. Margaritis, Mechanism for action of electromagnetic fields on cells, Biochem. Biophys. Res. Commun. 298 (1) (2002) 95–102.
[71] S. Marquez-Gamino, F. Sotelo, M. Sosa, C. Caudillo, G. Holguin, M. Ramos, F. Mesa, J. Bernal, T. Cordova, Pulsed electromagnetic fields induced femoral metaphyseal bone thickness changes in the rat, Bioelectromagnetics 29 (5) (2008) 406–409.